

Study of a model of a satellite structure that meets the necessary criteria for stability and rotation in space

Mahmoud Fadhel Idan, Osamah Mahmood Hussein

Department of Civil Engineering, University of Al Maarif, Al-Ramadi, Iraq

Article Info

Article history:

Received Nov 11, 2024

Revised Apr 25, 2025

Accepted May 10, 2025

Keywords:

Development

Geosynchronous orbit

Hexagonal structural

Satellite structure

Stability of satellite

ABSTRACT

The study aimed to create a model of a satellite structure that meets the necessary criteria for stability and rotation in space. The satellite being analyzed has an octagonal shape, with a diameter of 110 cm and a height of 85 cm. A dynamic modeling approach was used to analyze the structural properties, and the finite element method (FEM) was employed for computational analysis. This method allowed for a comprehensive evaluation of stress, displacement, and vibration distribution throughout the structure, providing insight into the behavior of the communications satellite in space. The test model frame consists of plates and bars arranged in an octagonal shape. The analysis utilized the von Mises stress (σ_vM) criterion to assess the yield strength or brittleness of the chosen material, 7,057 aluminum alloy. The study revealed that the structure demonstrates stability in six different modes but also exhibits deformation due to modifications in the basic arrangement. Additionally, transient fluctuations in the spacecraft's position over a 24-hour cycle result in changes in torque. The structure remains stable within a specified frequency range starting at 150 Hz when subjected to vibration stimuli, and no external instability was detected within this range.

This is an open access article under the [CC BY-SA](#) license.



Corresponding Author:

Mahmoud Fadhel Idan

Department of Civil Engineering, University of Al Maarif

Al-Ramadi, Anbar Province, Iraq

Email: dr.mafa57@gmail.com

1. INTRODUCTION

The development of a space system entails a thorough evaluation of its operating environment to ensure optimal performance, durability, and longevity of the satellite [1]. Natural alignment is especially critical in space because of the attendant challenges and expenses associated with the repair. For the current investigation, the spatial environment under study relates to the near-earth extension, which includes a range of altitudes ranging from low-earth orbit to geosynchronous orbit and beyond, including all possible inclinations [2], [3]. The complex and ever-changing natural space environment (SE) near earth can be described as a dynamic phenomenon. The outline and characterization of earth's features are influenced by several components, including the earth's natural geochemical properties, active intelligence between the earth and the sun, and multiple events in the interstellar and planetary space field [4]. The different interactions with space systems result in a wide range of effects [5]. These effects are divided into natural and artificial categories and are classified based on the variables of the SE [6]. When following the presentation strategy, a set of natural factors and their effects on near-earth space are presented in Table 1 [7]. In addition, guidance systems are used within the satellite or shuttle to correct its orientation, as mentioned in [8]–[10]. The motion of the satellite, affected by gravity and other forces, is complex. It is important to develop a diagram of the transient behavior of the relevant forces [5]–[19]. In 2010, he briefly presented a valuable

reflection on the effect of normal torque on the implementation of node number (N)-10 thrust tires in orbital elements [20]. References for modeling accurate gravitational reversal and radiative weight based on the sun can be obtained from sources 3, 4, and 5. A satellite is not an insignificant concentration of mass in studying the exploration of a planetary body, as already accepted by Kepler [21]. Normally, the shuttle is subjected to characteristic torques that affect its operation [22]–[24]: gravity ramp torque, sunbeam weight torque, gravity torque, airflow, heat probe, and pulse thrust torque. Low earth orbit (LEO) is a SE that poses various hazardous elements, including but not limited to atomic oxygen, ultraviolet radiation, and ionizing radiation consisting of electrons and protons, high vacuum, plasma, micrometeorites, debris, and fluctuations in degrees of heat [25]–[30]. Spacecraft exterior surfaces are subject to various environmental stresses that can degrade their building materials. One topic of current interest is the impact of the natural spatial environment on spacecraft design, development, and operations. In 2018, Nakka *et al.* studied a robotic spacecraft simulation platform called M-STAR to evaluate configuration orientation, relative navigation, and control algorithms [18]. The simulation functions with frictionless translational and rotational motion, alongside gravity-driven flight-like engines [31]–[33]. A 2019 study presented a theoretical framework for analyzing the dynamics of a tethered satellite system. It includes symmetrical rigid structures, balanced anchor points, and tethering to minimize weight [34]. Satellites approaching the end of their service life can be refurbished with imminent capabilities [35]. The revival of an unused satellite was enabled by Northrop Grumman's mission extension vehicle-1 (MEV-1), marking a new era of sustainable orbital utilization and advancing research in computer simulation of satellite infrastructure, envisioning it in a SE. The system's structural integrity is influenced by varying moments from different directions. This study aims to improve the geometric properties and moment of inertia for enhanced stability and rotation during space transit.

Table 1. SE and its impact on the space system [7]

Environmental factor	Effects
Earthshine and sunlight	Power, photo-mission, torque, drag, material damage, thermal cycling, and heating
Gravity	Torques and acceleration
Neutral atmosphere	Drag, torques, high vacuum, vacuum contamination, drag, and material degradation
System generated	System dependent: plasma, neutrals, plasma, forces, fields, particles, radiation, and torques

The study aimed to develop a stable octagonal satellite structure using dynamic modeling and finite element analysis and evaluate stress, displacement, and vibration throughout the design process. In addition, it sought to optimize the geometric properties and moment of inertia to ensure that the satellite meets the necessary criteria for stability and rotation during space travel. The research question in this study is “How can a stable octagonal satellite structure be developed using dynamic modeling and finite element analysis by evaluating stress, displacement, and vibration throughout the design process?”. The research innovations in this study are satellite designs that have focused primarily on cylindrical and cubic shapes. We studied the octagon to explore the potential of the octagon.

2. RESEARCH METHOD

2.1. Satellite structure representation

To simulate a communications satellite operating in a circular low earth orbit under SE conditions, we used a computational analysis technique called the finite element method (FEM) to thoroughly examine stress, strain, and vibration throughout the entire satellite structure. The frame substructure in the SE undergoes varying degrees of torque stress from multidirectional forces during the computational simulation. To accomplish this, we designed a test model in the shape of an octagon with a diameter of 110 cm and a height of 85 cm, as shown in Figure 1. Figure 2, contains a legend that illustrates the number of elements and nodes in the proposed satellite structure, including the connection points between them. We analyzed the structural properties by employing a dynamic modeling approach, using FEM as the computational analysis method. MSC Nastran software was used for static and dynamic analyses, and analyses for structural optimization, fatigue, and vibration using FEMs. This approach enabled a comprehensive investigation of the allocation of stress, fatigue, and vibration throughout the structure. The test model frame is represented as a right octagon of plates and bars, with the plate being represented by a four-node quadrilateral element. The structure consists of three bases: upper, middle, and lower. Each base includes four plate elements, eight peripheral nodes, and one central node. Additionally, each rod is represented by a two-node element. The upper and lower bases each consist of eight elements, while the middle base is reinforced with two additional bars. There are two rods at the middle base, with the first connecting knot 11 to central knot 25 and the second connecting knot 15 to central knot 25. Eight rods connect the upper base to the middle base, and another eight connect the lower base to the middle base. The first rod at the middle base connects knot 27 to knot 25, and the second crossbar connects knot 25 to knot 26. A plate is a four-sided plane with uniform

thickness. All elements, from plates to bars, have the same physical properties. Each node has six degrees of freedom, three translational and three rotational. The origin is located in the middle of the body at node 25. This gives the amount of 27 nodes (N) and 54 elements (NE), with 12 elements representing plates and 42 elements representing rods. Figure 1 illustrates the distribution of panels, bars, and nodes on the frame. To adequately meet the requirements of these loads, it is recommended to use the von Mises stress (σ_vM) criterion to assess the yield capacity or brittleness of the material. The experimental prototype will be fabricated using 7,057 aluminum alloy, chosen for its noteworthy mechanical properties, including a tensile strength of 572 MPa and yield strength of 503 MPa.

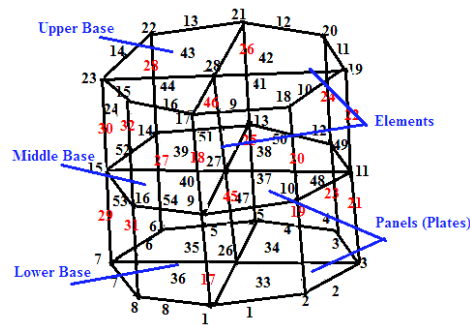


Figure 1. Satellite architecture with modeling analysis

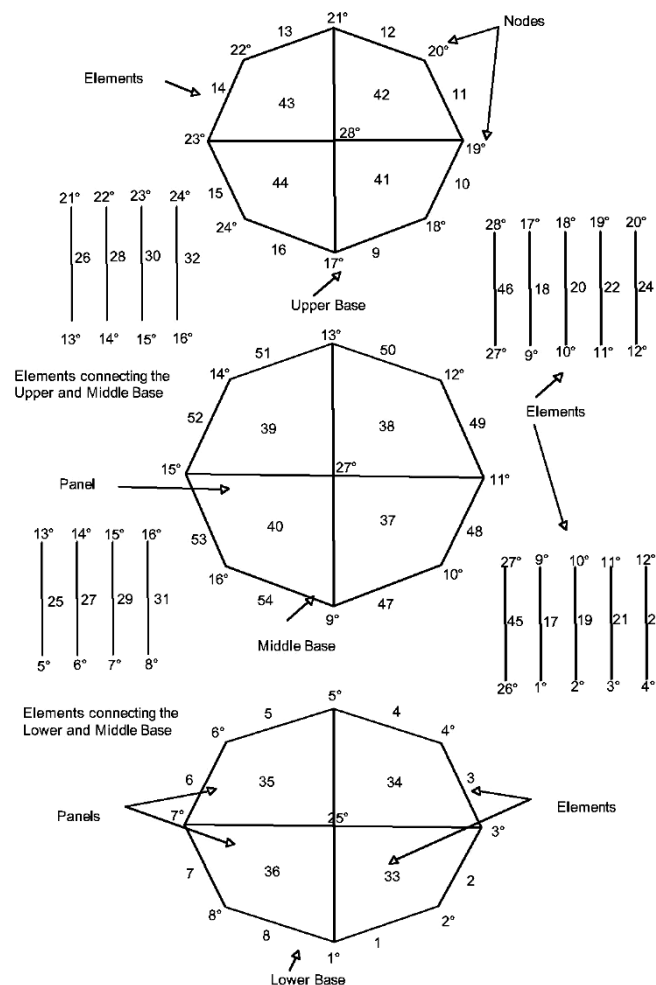


Figure 2. A legend that displays the number of elements and nodes in the proposed satellite structure and the connection points between them

2.2. Representation of loads on the satellite structure

The prototype's steering and handling will be controlled using 10 N motors, known for their low levels of thrust. The pulse duration is typically short, with a minimum of 0.3 seconds. To analyze the stresses and deformations of the structure, we determined and classified the loads as internal and external. The internal loads represent the payloads, such as the communication antenna installed at node 27, the compressed air tank to supply the thrusters in the air, and the energy storage battery installed between points 25 and 27 to supply electrical power to the satellite in the dark area. Furthermore, the control systems are represented by two thrust motors (10 N) installed in nodes 14 and 18 in the x direction, and two more installed in nodes 2 and 6 in the y direction, to handle internal loads and for movement and maneuvering. External loads include gravitational forces from the earth, sun, and other planets, as well as air pressure. These external loads can be represented by a torque that affects all nodes equally, with a torque of 1 Nm. The total torque of the external load group is less than 1 Nm. To assess the stress and deformation capabilities of the intended satellite construction, an investigation was conducted on different classes of loads to which the prototype is subjected to SE testing. Conventional analysis was carried out to determine the frequencies and modes corresponding to the structure, along with their corresponding modes. In the field of static analysis, the observed displacement caused by the applied load was calculated. Furthermore, the method used for static analysis included the calculation of component forces, stresses, and interaction forces. An examination was conducted to study the effect of an applied torque of 1 Nm on the distribution of σ_vM along the X and Y coordinates of the structure to cope with the external loads. Furthermore, the effects of the applied torque of 10 N on the distribution of σ_vM along the X and Y coordinates of the structure were studied to address internal loads, maneuver, and complete the tasks assigned to the proposed satellite.

2.3. Properties of 7,075 aluminum alloy

Aluminum type 7,075 is one of the strongest aluminum alloys [36]–[38]. Its high yield strength and low density make the material suitable for applications such as aircraft parts or parts subject to heavy corrosion aircraft fittings. The composition of 7,075 aluminum alloy roughly includes 5.6-6.1% zinc, 2.1-2.5% magnesium, 1.2-1.6% copper, and less than half a percent silicon, iron, manganese, titanium, chromium, and other metals [37]. Its density is 2.81 g/cm^3 , which is relatively light for a metal. 7,075 aluminum is one of the strongest aluminum alloys available, making it valuable in high-stress situations. The copper content in 7,075 aluminum increases its susceptibility to corrosion. A material's resistance to deformation is determined by its modulus of elasticity and shear modulus. The modulus of elasticity for 7,075 aluminum is 71.7 GPa, and the shear modulus is 26.9 GPa (see Table 2) [38], [39]. One of the most important measures is its yield strength. The yield strength of a material is defined as the maximum amount of stress (or force over an area) that will not permanently deform the material. The yield strength of 7,075 aluminum is 503 GPa [36].

Table 2. Mechanical properties of 7,075 aluminum alloy [36]

Mechanical properties	Measurement (MPa)
Tensile strength	572
Yield tensile strength	503
Shear strength	331
Fatigue strength	159
Modulus of elasticity	71.7
Shear modulus	26.9

2.4. Von Mises criterion

The σ_vM stress criterion simplifies stress analysis by providing a single value that summarizes the total stress intensity, regardless of direction. For evaluating materials under multi-axial stress, this effectively captures the combined effects of multiple stresses at a single point. This capability enhances the safety and reliability of structures and products, making it essential for stress analysis in satellite structures.

The σ_vM is calculated using the (1).

$$\sigma_{vM} = \sqrt{(\sigma_x - \sigma_y)^2 + (\sigma_y - \sigma_z)^2 + (\sigma_z - \sigma_x)^2 + 6(\tau_{xy}^2 + \tau_{yz}^2 + \tau_{zx}^2)} \quad (1)$$

In this context, σ_x , σ_y , and σ_z represent the normal stresses in the x, y, and z directions, while τ_x , τ_y , and τ_z denote the shear stresses in the respective x, y, and z planes.

3. RESULTS AND DISCUSSION

The results obtained from the analysis are shown in Table 3 and Figures 3-24. Table 3 shows the eigenvectors and their corresponding modes, which are similar to the fixed displaced features in Figure 3. The highest distortion values are found in modes 6 and 5, with distortion values of 0.0544 and 0.0488 m, respectively, at eigenvectors of 187.85904 and 178.6357 Hz. In stability analysis, observed displacement refers to the physical displacement resulting from an applied load. This study explores the effect of an applied torque of 1 N on the dispersion of $\sigma_v M$ across the X and Y axes. Figures 4-6 illustrate the values of $\sigma_v M$ within different structural components, examining the stress distribution due to the torque. The observed displacement values at the characteristic nodes of the structure, along with their corresponding X and Y coordinates under a 1 N torque, are shown in Figures 7-9. Furthermore, Figures 10-15 display the current values of $\sigma_v M$ within different structural components of the system, along with their corresponding distributions. These stress values were obtained while the system was subjected to a thrust load of 10 N in both the X and Y directions. Figures 16-21 display the displacement magnitudes of various nodes at the X and Y coordinates of the structure. These measurements were taken while subjecting the structure to a thrust load of 10 N in both directions. Based on the experimental findings, it is evident that stress diffusion results in a significant increase in stress levels on the bottom plate of element 34 compared to other plate and rod elements. The hinge positions are of particular interest, with a recorded $\sigma_v M$ of 314.714 N/m². Additionally, both the hinges and the body panel experienced extreme stress levels of 4,423 N/m². When a specific architectural structure is subjected to a driving force in the x-axis, the component exhibiting the highest stress level is component 49, while the stress level is lower in element 38 due to its plate-type nature, in contrast to the strip element number (NE) 49. The results above demonstrate how external forces interact with the structure, guiding design and technological applications. When the thrust load is applied in the y direction, element 42 experiences the highest stress, while element 49 experiences the lowest stress within the structure. Additionally, the maximum displacement occurs at node 4 in two different directions. There is a noticeable difference in stress levels between items 1-32 and 33-54, which is attributed to their structural characteristics-the former consists of rods, and the latter consists of sheet structures. This result emphasizes the critical role that the inherent structural properties of materials play in determining their stress response. The proposed satellite is subjected to environmental loads from acceleration in a space field. To determine the displacements and stresses experienced by the nodes and characteristic elements under variable loads, transient response analysis using the FEM configuration model followed by load application is necessary. Figure 22 visually represents the relationship between displacement and time, while the stress distribution is investigated. The investigation illustrates the $\sigma_v M$ in various components, as shown in Figure 23. The structure was subjected to a frequency range of 0 to 200 Hz, with an additional step of 1 Hz. Figure 24 provides a graphical representation of the relationship between displacement and frequency.

Table 3 Output sums for each case, the modal value in hertz, and the total distortion at that frequency

Case number	Eigenvectors (Hz)	Total distortion (cm)
1	1.93559	0.0405
2	3.49003	0.0407
3	46.62015	0.0591
4	49.28521	0.0625
5	178.6357	0.0488
6	187.85904	0.0544

3.1. Practical implications

The Nastran software was used for dynamic modeling and finite element analysis in this study. The research focused on developing a stable octagonal satellite structure, with an emphasis on enhancing its mechanical properties and torque characteristics. This was essential to ensure structural stability and precise rotational behavior in the space environment. The design process also considered the harsh environmental conditions encountered in space, which helped improve the satellite's reliability and operational performance.

3.2. Theoretical implications

The analysis of mechanical structures under various loading conditions primarily depends on static and dynamic principles to evaluate stresses, displacements, and natural frequencies. While this analytical process can be time-consuming, the use of Nastran significantly enhances both computational accuracy and efficiency. This advancement is crucial for managing complex structures, such as satellites, as it enables real-time results that accurately reflect their behavior. Ultimately, this improvement increases the theoretical and practical significance of the analysis.

3.3. Limitations of the study

A significant limitation of this study is the necessity to accurately specify the input data for each element, node, and panel within the Nastran software, particularly concerning the loads and moments applied to the satellite structure. While the software facilitates easy modifications of loads and dimensions, any inaccuracies or assumptions in these inputs could negatively affect the simulation's accuracy.

3.4. Limits of scientific research

This study focuses on the design of an octagonal low-earth orbit communications satellite, using the Nastran modeling software. It does not include field tests or practical applications. The applied loads and environmental conditions are based on theoretical parameters and do not address long-term effects or satellite lifetime. The analysis is based on specific materials, assuming constant mechanical properties, and excludes considerations of material defects, degradation, and harsh environmental factors that could affect performance and reliability.

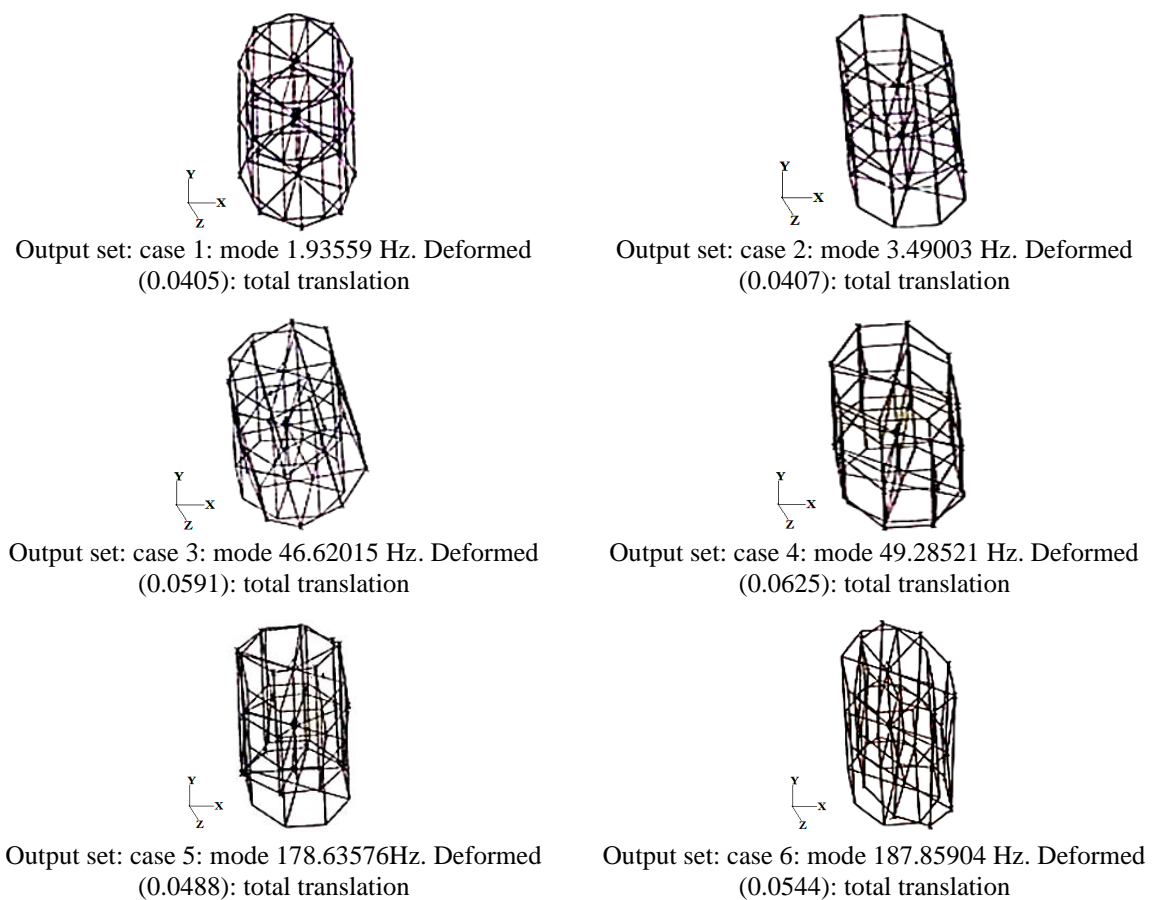


Figure 3. Structure mode shapes

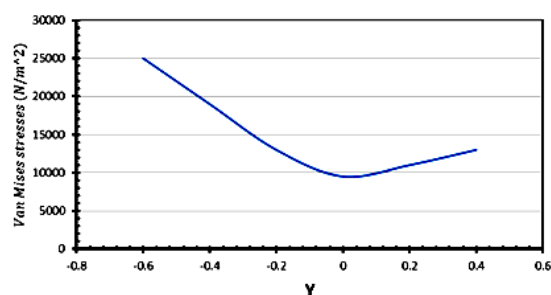


Figure 4. The relationship between the values σ_M of and its position in the Y direction

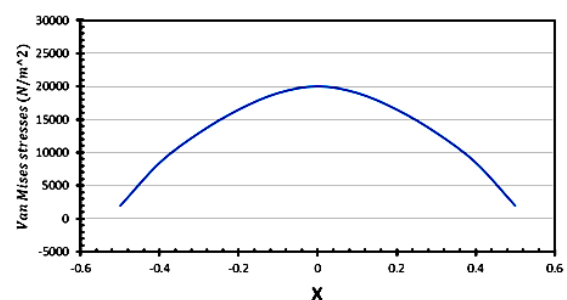


Figure 5. The relationship between the values of σ_M and its position in the X direction

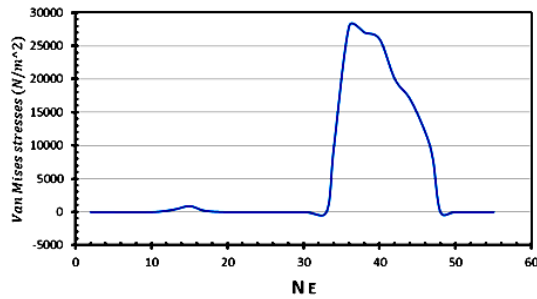


Figure 6. The relationship between the values of $\sigma_v M$ and its NE

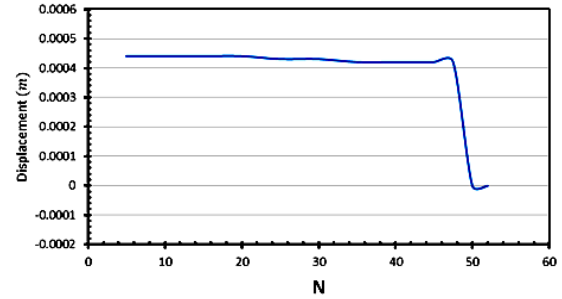


Figure 7. The relationship between displacement values and its N

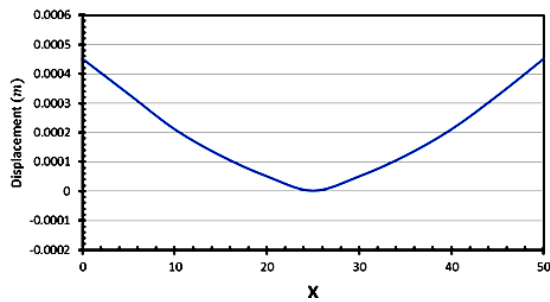


Figure 8. The relationship between displacement values and its position in the X direction

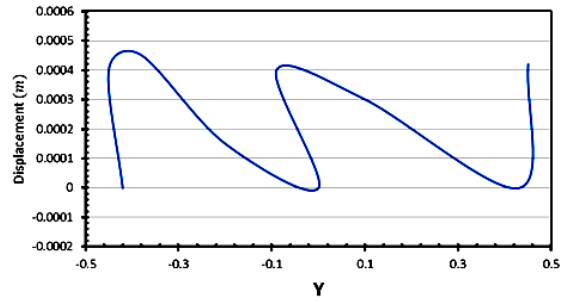


Figure 9. The relationship between displacement values and its position in the Y direction

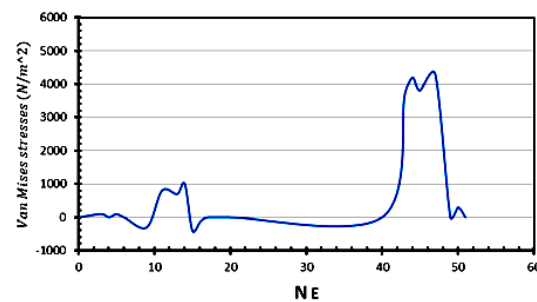


Figure 10 The relationship between $\sigma_v M$ values and its NE at load thruster load in X-the direction (TX)

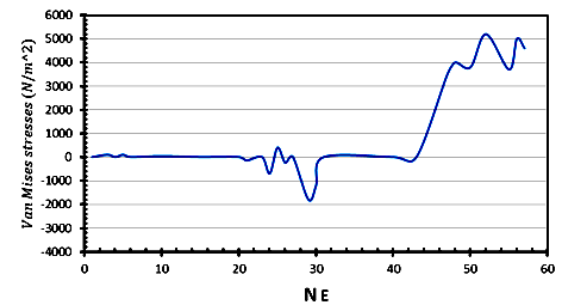


Figure 11. The relationship between $\sigma_v M$ values and its NE at load thruster load in Y-the direction (TY)

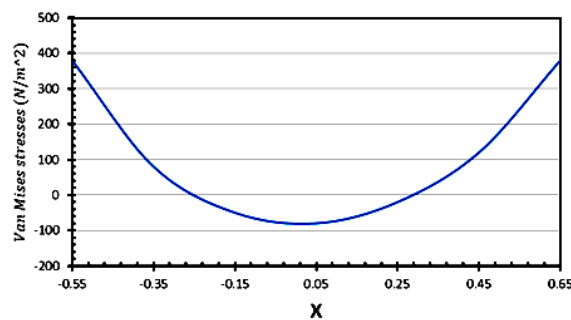


Figure 12. The relationship between $\sigma_v M$ values and X at load TX

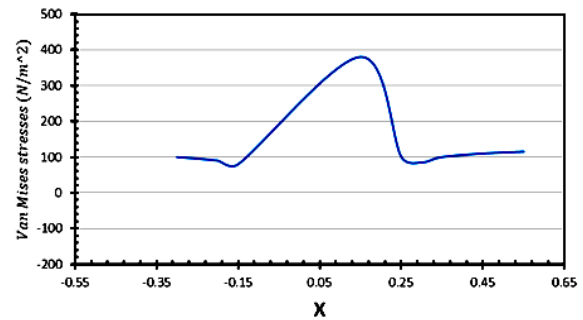


Figure 13. The relationship between $\sigma_v M$ values and X at load TY

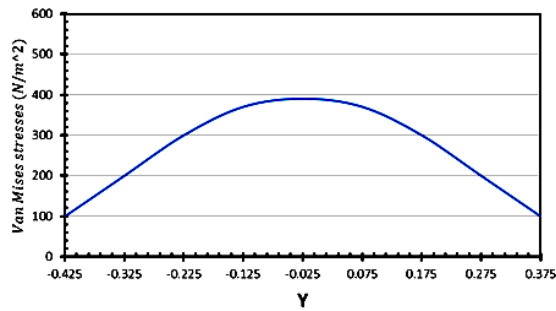


Figure 14. The relationship between $\sigma_v M$ values and Y at load TX

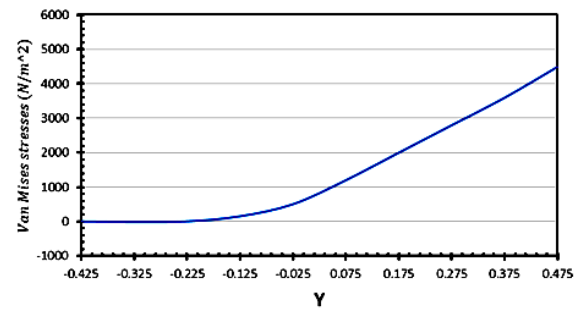


Figure 15. The relationship between $\sigma_v M$ values and Y at load TY

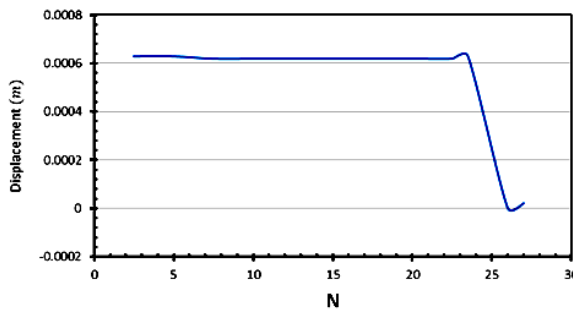


Figure 16. The relationship between displacement values and N at load TX

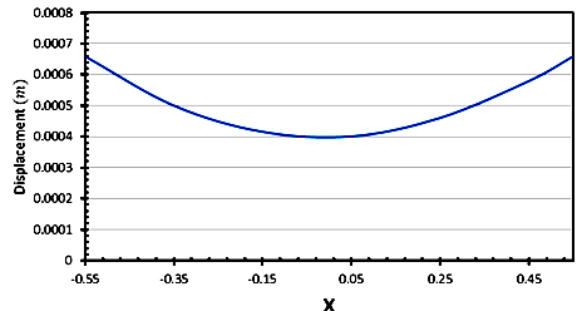


Figure 17. The relationship between displacement values and X at load TX

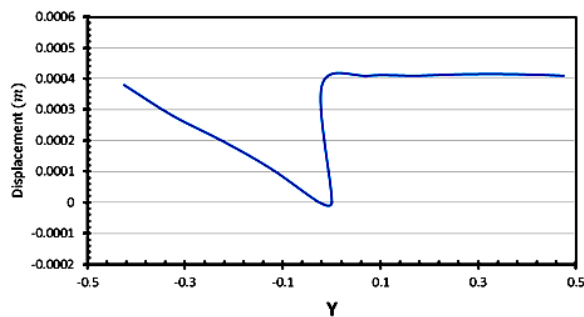


Figure 18. The relationship between displacement values and Y at load TX

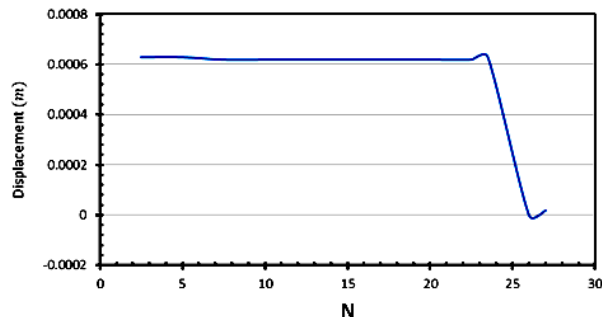


Figure 19. The relationship between displacement values and N at load TY

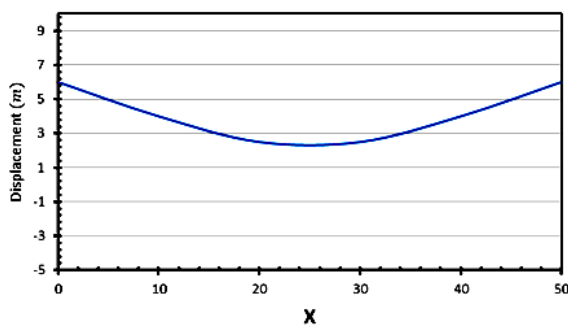


Figure 20. The relationship between displacement values and X at load TY

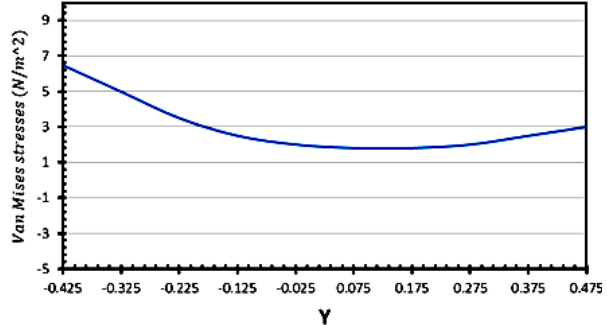


Figure 21. The relationship between displacement values and Y at load TX

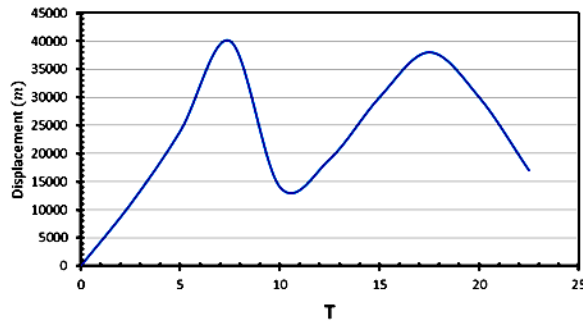


Figure 22. The relationship between displacement values and time

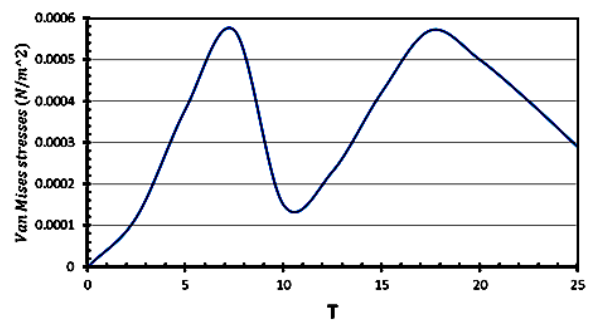


Figure 23. The relationship between the $\sigma_v M$ value and time

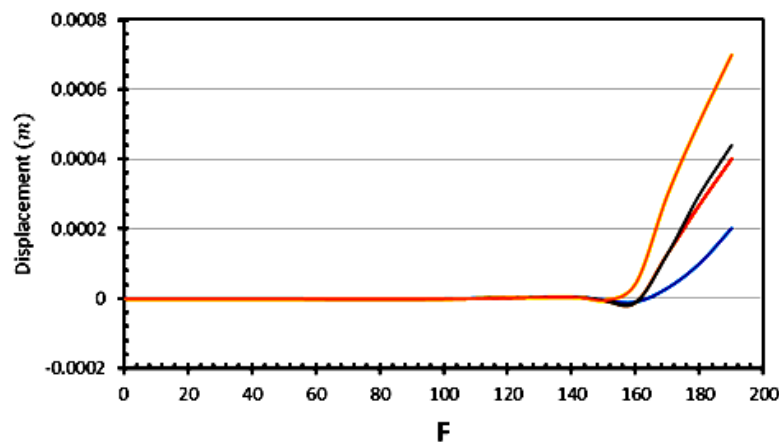


Figure 24. The relationship between displacement values and frequency

4. CONCLUSION

The operational parameters have been obtained and approved for use in SE conditions. Passive and dynamic investigations have revealed several additional benefits for their use in structural design and useful load distribution. The near-earth environment constantly changes and involves various components significantly affected by relevant frames. Based on the frame position values, it can be concluded that the structure maintains stability in up to six specific positions, which exhibit slight deformation due to changes in the arrangement of the upper and lower bases. The significant displacement of the lower plate under a 10 N thrust at element 33, along with the concentrated thrust on the driven component of element 41, makes using a driven pile on the upper and lower plates impractical. The $\sigma_v M$ magnitude is significantly lower than the yield stress of 7,075 aluminum alloy, indicating that the structure is safe. The spacecraft's torque undergoes transient changes due to its position changes over 24 hours. The structure is stable during vibration within a frequency range of 150 Hz, with no external instability observed. Examine different satellite structures-circular, quadrilateral, pentagonal, and hexagonal evaluate stability, rotation, stress distribution, displacement, and vibrations optimal design.

ACKNOWLEDGMENTS

The researchers would like to thank the Deanship and professors of the College of Engineering for the great support and encouragement they provided to complete the research.

FUNDING INFORMATION

Authors state no funding involved.

AUTHOR CONTRIBUTIONS STATEMENT

This journal uses the Contributor Roles Taxonomy (CRediT) to recognize individual author contributions, reduce authorship disputes, and facilitate collaboration.

Name of Author	C	M	So	Va	Fo	I	R	D	O	E	Vi	Su	P	Fu
Mahmoud Fadhel Idan	✓	✓	✓		✓	✓	✓		✓	✓		✓	✓	
Osamah Mahmood Hussein		✓	✓		✓			✓	✓	✓				

C : Conceptualization

M : Methodology

So : Software

Va : Validation

Fo : Formal analysis

I : Investigation

R : Resources

D : Data Curation

O : Writing - Original Draft

E : Writing - Review & Editing

Vi : Visualization

Su : Supervision

P : Project administration

Fu : Funding acquisition

CONFLICT OF INTEREST STATEMENT

Authors state no conflict of interest.

DATA AVAILABILITY

The data that support the findings of this study are available from the corresponding author, [MFI], upon reasonable request.




REFERENCES

- [1] J. E. Lavín-Delgado, S. Chávez-Vázquez, J. F. Gómez-Aguilar, M. O. Alassafi, F. E. Alsaadi, and A. M. Ahmad, "Intelligent neural integral sliding-mode controller for a space robotic manipulator mounted on a free-floating satellite," *Advances in Space Research*, vol. 71, no. 9, pp. 3734–3747, May 2023, doi: 10.1016/j.asr.2022.08.053.
- [2] M. Deveci, D. Pamucar, I. Gokasar, and M. Tavana, "Spacecraft tracking control and synchronization: an assessment of conventional, unconventional, and combined methods," *Advances in Space Research*, vol. 71, no. 9, pp. 3534–3551, May 2023, doi: 10.1016/j.asr.2022.07.056.
- [3] K. K. de Groh, B. A. Banks, S. K. R. Miller, and J. A. Dever, "Degradation of spacecraft materials," in *Handbook of Environmental Degradation of Materials*, Elsevier, pp. 601–645, 2018, doi: 10.1016/B978-0-323-52472-8.00029-0.
- [4] Y. Lu, Q. Shao, H. Yue, and F. Yang, "A review of the space environment effects on spacecraft in different orbits," *IEEE Access*, vol. 7, pp. 93473–93488, 2019, doi: 10.1109/ACCESS.2019.2927811.
- [5] J. L. Ramón, J. Pomares, and L. Felicetti, "Direct visual servoing and interaction control for a two-arms on-orbit servicing spacecraft," *Acta Astronautica*, vol. 192, pp. 368–378, Mar. 2022, doi: 10.1016/j.actaastro.2021.12.045.
- [6] B. F. James, O. W. Norton, and M. B. Alexander, "The natural space environment: effects on spacecraft," 1994. [Online]. Available: <https://ntrs.nasa.gov/api/citations/19950019455/downloads/19950019455.pdf>
- [7] I. Kolmanovsky and M. Ilić, "Control of aerospace systems," *Annual Reviews in Control*, vol. 52, pp. 280–281, 2021, doi: 10.1016/j.arcontrol.2021.10.011.
- [8] A. C. Boley and M. Byers, "Satellite mega-constellations create risks in low earth orbit, the atmosphere and on earth," *Scientific Reports*, vol. 11, no. 1, May 2021, doi: 10.1038/s41598-021-89909-7.
- [9] N. T. Redd, "Bringing satellites back from the dead: mission extension vehicles give defunct spacecraft a new lease on life - [news]," *IEEE Spectrum*, vol. 57, no. 8, pp. 6–7, Aug. 2020, doi: 10.1109/MSPEC.2020.9150540.
- [10] M. N. Ross and K. L. Jones, "Implications of a growing spaceflight industry: climate change," *Journal of Space Safety Engineering*, vol. 9, no. 3, pp. 469–477, Sep. 2022, doi: 10.1016/j.jsse.2022.04.004.
- [11] R. Xu, J. Luo, and M. Wang, "Kinematic and dynamic manipulability analysis for free-floating space robots with closed chain constraints," *Robotics and Autonomous Systems*, vol. 130, Aug. 2020, doi: 10.1016/j.robot.2020.103548.
- [12] Z. Wang, R. M. Jungers, M. Petreczky, B. Chen, and L. Yu, "Learning stability of partially observed switched linear systems," *Automatica*, vol. 164, Jun. 2024, doi: 10.1016/j.automatica.2024.111643.
- [13] B. M. Moghaddam and R. Chhabra, "On the guidance, navigation and control of in-orbit space robotic missions: a survey and prospective vision," *Acta Astronautica*, vol. 184, pp. 70–100, Jul. 2021, doi: 10.1016/j.actaastro.2021.03.029.
- [14] H. Tsukamoto, S.-J. Chung, and J.-J. E. Slotine, "Contraction theory for nonlinear stability analysis and learning-based control: a tutorial overview," *Annual Reviews in Control*, vol. 52, pp. 135–169, 2021, doi: 10.1016/j.arcontrol.2021.10.001.
- [15] X. Zhang, Y. Geng, and B. Wu, "Approaching and pointing tracking control for tumbling target under motion constraints," *Acta Astronautica*, vol. 209, pp. 6–20, Aug. 2023, doi: 10.1016/j.actaastro.2023.04.025.
- [16] R. Jin, P. Rocco, and Y. Geng, "Observer-based fixed-time tracking control for space robots in task space," *Acta Astronautica*, vol. 184, pp. 35–45, Jul. 2021, doi: 10.1016/j.actaastro.2021.04.002.
- [17] C. Nieto-Peroy, M. Sabatini, G. Palmerini, and É. Jeronimo de Oliveira, "A concurrent testing facility approach to validate small satellite combined operations," *Aerospace*, vol. 8, no. 12, p. 361, Nov. 2021, doi: 10.3390/aerospace8120361.
- [18] Y. K. Nakka *et al.*, "A six degree-of-freedom spacecraft dynamics simulator for formation control research," in *2018 AAS/AIAA Astrodynamics Specialist Conference*, AIAA, 2018. [Online]. Available: https://authors.library.caltech.edu/records/r1424-xmc64/files/2018_AAS_AIAA.pdf?download=1
- [19] W. Zhang and H. Wen, "Motion planning of a free-flying space robot system under end effector task constraints," *Acta Astronautica*, vol. 199, pp. 195–205, Oct. 2022, doi: 10.1016/j.actaastro.2022.07.005.
- [20] M. Yu, J. Luo, M. Wang, J. Li, C. Liu, and J. Sun, "Directly skill-transferred DMP-based trajectory planning for robot soft-capture of space tumbling targets," *Acta Astronautica*, vol. 204, pp. 611–629, Mar. 2023, doi: 10.1016/j.actaastro.2022.11.043.




- [21] P. Rousso and R. Chhabra, "Singularity-robust full-pose workspace control of space manipulators with non-zero momentum," *Acta Astronautica*, vol. 208, pp. 322–342, Jul. 2023, doi: 10.1016/j.actaastro.2023.04.022.
- [22] A.-Y. Huang and H.-N. Li, "Simplified optimization model for low-thrust perturbed rendezvous between low-eccentricity orbits," *Advances in Space Research*, vol. 71, no. 11, pp. 4751–4764, Jun. 2023, doi: 10.1016/j.asr.2023.01.016.
- [23] J. Garcia, D. Gonzalez, A. Rodriguez, B. Santamaria, J. Estremera, and M. Armendia, "Application of impedance control in robotic manipulators for spacecraft on-orbit servicing," in *2019 24th IEEE International Conference on Emerging Technologies and Factory Automation (ETFA)*, IEEE, pp. 836–842, Sep. 2019, doi: 10.1109/ETFA.2019.8869069.
- [24] J. Peng, W. Xu, B. Liang, and A.-G. Wu, "Virtual stereovision pose measurement of noncooperative space targets for a dual-arm space robot," *IEEE Transactions on Instrumentation and Measurement*, vol. 69, no. 1, pp. 76–88, Jan. 2020, doi: 10.1109/TIM.2019.2893010.
- [25] S. Yang, W. Zhang, Y. Zhang, H. Wen, and D. Jin, "Development and evaluation of a space robot prototype equipped with a cable-driven manipulator," *Acta Astronautica*, vol. 208, pp. 142–154, Jul. 2023, doi: 10.1016/j.actaastro.2023.04.014.
- [26] M. F. Idan, "Simulation the effect of vibroacoustic on space vehicle structures," *Journal of Engineering and Applied Sciences*, vol. 15, no. 8, pp. 1962–1971, 2020, doi: 10.36478/jeasci.2020.1962.1971.
- [27] A. Nishimura and K. Tsujita, "An experimental maneuver control for rendezvous and autonomous docking of a small spacecraft," *SICE Journal of Control, Measurement, and System Integration*, vol. 16, no. 1, pp. 98–108, Dec. 2023, doi: 10.1080/18824889.2023.2187163.
- [28] A. V. Moorhead, A. Kingery, and S. Ehlert, "NASA's meteoroid engineering model 3 and its ability to replicate spacecraft impact rates," *Journal of Spacecraft and Rockets*, vol. 57, no. 1, pp. 160–176, Jan. 2020, doi: 10.2514/1.A34561.
- [29] A. Rossi, A. Petit, and D. McKnight, "Short-term space safety analysis of Leo constellations and clusters," *Acta Astronautica*, vol. 175, pp. 476–483, Oct. 2020, doi: 10.1016/j.actaastro.2020.06.016.
- [30] R. Massey, S. Lucatello, and P. Benvenuti, "The challenge of satellite megaconstellations," *Nature Astronomy*, vol. 4, no. 11, pp. 1022–1023, Nov. 2020, doi: 10.1038/s41550-020-01224-9.
- [31] A. Venkatesan, J. Lowenthal, P. Prem, and M. Vidauri, "The impact of satellite constellations on space as an ancestral global commons," *Nature Astronomy*, vol. 4, no. 11, pp. 1043–1048, Nov. 2020, doi: 10.1038/s41550-020-01238-3.
- [32] Z. Zhang, X. Li, J. An, W. Man, and G. Zhang, "Model-free attitude control of spacecraft based on PID-guide TD3 algorithm," *International Journal of Aerospace Engineering*, vol. 2020, pp. 1–13, Dec. 2020, doi: 10.1155/2020/8874619.
- [33] J. Gibart, H. Piet-Lahanier, F. Farago, and M. Galeotta, "Regulation of a liquid propelled rocket engine using contraction theory," *IFAC-PapersOnLine*, vol. 56, no. 1, pp. 307–312, 2023, doi: 10.1016/j.ifacol.2023.02.052.
- [34] M. Kocifaj, F. Kundracik, J. C. Barentine, and S. Bará, "The proliferation of space objects is a rapidly increasing source of artificial night sky brightness," *Monthly Notices of the Royal Astronomical Society: Letters*, vol. 504, no. 1, pp. L40–L44, Apr. 2021, doi: 10.1093/mnrasl/slab030.
- [35] Z. Huang, W. Zhang, T. Chen, H. Wen, and D. Jin, "Characterizing an air-bearing testbed for simulating spacecraft dynamics and control," *Aerospace*, vol. 9, no. 5, May 2022, doi: 10.3390/aerospace9050246.
- [36] B. P. Malladi, R. G. Sanfelice, and E. A. Butcher, "Robust hybrid supervisory control for spacecraft close proximity missions," *Annual Reviews in Control*, vol. 52, pp. 316–329, 2021, doi: 10.1016/j.arcontrol.2021.11.001.
- [37] Aerospace Specification Metals Inc., "Aluminum 2024-T3," *satsearch B.V.*, 2024. [Online]. Available: <https://satsearch.co/suppliers/aerospace-specification-metals-inc>
- [38] R. F. Muraca and J. S. Whittick, "Materials data handbook: aluminum alloy 7075," 1972. Accessed: Dec. 01, 2024. [Online]. Available: <https://ntrs.nasa.gov/citations/19720022809>
- [39] Gabrian Team, "7075 aluminum: get to know its properties and uses," Gabrian International. Accessed: Dec. 04, 2024. [Online]. Available: <https://www.gabrian.com/7075-aluminum-properties/>

BIOGRAPHIES OF AUTHORS



Mahmoud Fadhel Idan    holds a Ph.D. in Mechanical Engineering from the University of Baghdad-Designs, 1997, a Master's degree in Mechanical Engineering-Applied Mechanics-University of Technology, 1982, Higher Diploma in Mechanical Engineering-Applied Mechanics-University of Technology, 1981 and Bachelor's Degree-Mechanical Engineering-University of Technology, 1979. He has conducted extensive research in space, physics, satellites, management, mechanical and civil engineering. He worked at the Space and Physics Research Center (BATANI CENTER) and taught at public and private universities. In addition, he has authored a book on total quality, which has been printed and published in several international languages. He can be contacted at email: dr.mafa57@gmail.com.



Osamah Mahmood Hussein    is PhD obtained a Master's in Civil Engineering from Al Nahrain University, Baghdad, Iraq, in 2013. He obtained a Bachelor's degree in Civil Engineering from Anbar University, Ramadi, Iraq, in 2010. He has many projects in the field of soil research and many projects in analysis, inspection, and design. He is proficient in preparing and operating various computer programs. He can be contacted at email: engosamah8896@gmail.com.